JOURNAL OF AIRCRAFT
Vol. 32, No. 5, September–October 1995

# Structural Modeling for Optimization of Low Aspect Ratio Composite Wings

L. Meirovitch* and T. J. Seitz†
*Virginia Polytechnic Institute and State University, Blacksburg, Virginia 24061*

**This article is concerned with the aeroelastic tailoring of a structural model consisting of a low aspect ratio wing made of composite materials and a rigid fuselage. The wing is modeled as a trapezoidal plate with root and tip chords parallel to the flow and with general sweep. The plate is made of symmetrically stacked, variable thickness, orthotropic laminae. The elastic wing model includes shear deformations and is attached to a rigid fuselage capable of plunge and pitch.**

## I. Introduction

THE main objective of this study is to develop a structural model for a low aspect ratio (AR) composite aircraft wing that includes all the essential features and at the same time is sufficiently simple to permit a multidisciplinary optimization. One such feature, widely ignored until now, consists of the pitch and plunge rigid-body degrees of freedom (DOFs) of the fuselage.

During the past decade, the problem of flutter of anisotropic wings made of composite materials has received a great deal of attention. Much of this work has been directed toward refining the concept of "composite tailoring." At the same time, many researchers have come to the conclusion that the divergence problem associated with forward-swept wings is in fact a body-freedom flutter phenomenon. Body-freedom flutter is the coupling of a flexible aircraft mode with a rigid-body mode due to interaction with aerodynamic loads. One common example of this, and the one receiving attention here, is the coupling of wing bending and rigid-body pitch. Work by Weisshaar et al.[1] leads to the conclusion that a clamped wing model generally predicts larger improvements in the instability speed for composite tailoring than for models including rigid-body motions. The capability of predicting accurately the critical speed in the presence of structural parameter variations is essential to any structural model of general planforms.

The requirements of modern wing planforms place additional constraints on structural models. In particular, the AR of many wings of practical interest tends to be too low to be approximated by a beam model. Similarly, the midchord sweep angle $\Lambda$ should not be confined to aft only, particularly for an optimization problem. Two-dimensional models with varying fiber orientation are suggested in this case, but examples of such models in the technical literature are rare.[2,3,15]

In view of the physical requirements discussed above, we consider a structural model consisting of a two-dimensional anisotropic plate made of several variable-thickness layers of generally orthotropic material. Because the interest lies in composite materials, it is also important to include shear deformability in the model. Whereas shear deformability is of minor importance in the case of some hollow wings, its inclusion is essential in the case of solid core structures, such as canards, cruise-missile components, and aeroelastic wind-tunnel models, for which this formulation is intended. Moreover, fuselage rigid-body DOFs must also be included. Two compromises on generality help toward the goal of low computational effort without significantly affecting the effort to include all the relevant physical effects. Realistic amounts of airfoil camber have little effect on displacements due to unsteady pressure loading, suggesting that camber can be omitted for aeroelastic problems. Similarly, rotatory inertia terms can be ignored for wings of practical thickness, as shown in the text by Librescu.[4]

The interest lies in a structural model incorporating the physical characteristics essential to a flutter analysis of modern low AR composite wings. The model should be sufficiently accurate to account for all important structural parameters and yet sufficiently simple so as not to be computationally intensive. Such a structural model consists of a trapezoidal plate with root and tip chords parallel to the flow and with $2k$ symmetrically stacked, variable thickness, generally orthotropic laminae in the laminate (Figs. 1 and 2). Mindlin shear deformability[5] is included with a shear correction factor (SCF) of 1.0. The wing is attached to a rigid fuselage capable of pitch and plunge. Note that the SCF generally appears as a proportionality factor in the coefficient $A_{ab}$ [Eq. (12)]. In the present parametric study, it was chosen arbitrarily as 1.0, but is to be replaced by an appropriate value in actual design. This is the simplest model retaining the essential physical

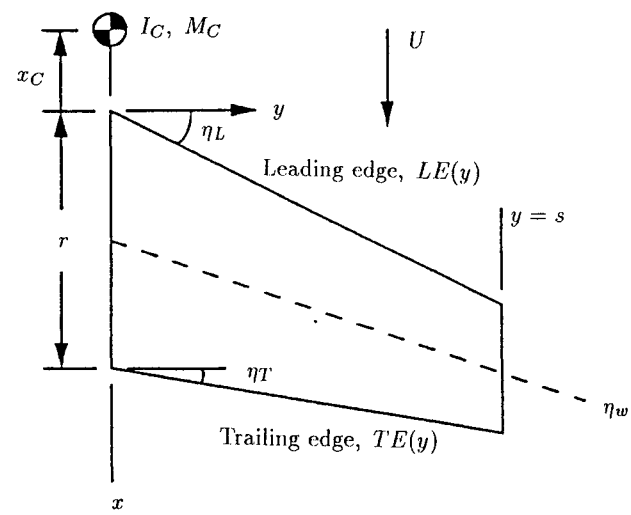


**Fig. 1 Planform.**

Received Oct. 21, 1993; revision received Feb. 27, 1995; accepted for publication Feb. 27, 1995. 

*University Distinguished Professor, Department of Engineering Science and Mechanics. Fellow AIAA.

†Graduate Research Assistant, Department of Engineering Science and Mechanics; currently Supervisor, Loads and Flutter, Cessna Aircraft Company, Wichita, KS 67215. Senior Member AIAA.

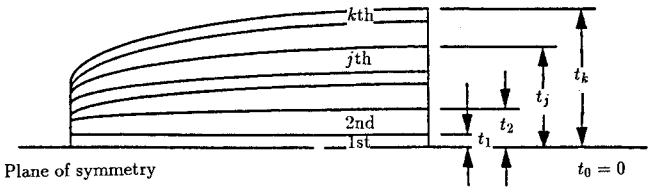


**Fig. 2 Laminate.**

characteristics of low AR composite wings with general sweep. It is still a relatively involved formulation, however, including three displacement variables and natural boundary conditions complicated by the leading- and trailing-edge sweep angle $\eta_L$ and $\eta_T$, respectively. To produce a reasonably accurate solution with as few terms as possible, the series solution is in terms of quasicomparison functions, which are shape functions guaranteeing fast convergence.[6]

## II. Definition of Displacements and Boundary Conditions

The mathematical model under consideration consists of a flexible wing attached to a rigid fuselage. The fuselage is assumed to undergo two rigid-body displacements, namely, plunge and pitch. On the other hand, the wing is assumed to act as an elastic plate rigidly attached at the root and free at the other three boundaries (Fig. 1). The transverse displacement of a typical point in the fuselage has the form

$$w_f(t) = w_C(t) + (x - x_C)\psi_C(t) \tag{1a}$$

where $w_C(t)$ is the plunge, defined as the transverse displacement of the system (fuselage and wing) mass center $C$, $\psi_C$ is the pitch, defined as the rotation of the system about an axis parallel to $y$ and passing through $C$, and $x_C$ is the distance from the origin of $xyz$ to point $C$. Moreover, the displacements of a typical point in the plate are as follows:

$$u(x, y, z, t) = u_0(x, y, t) + z\psi_x(x, y, t) \tag{1b}$$

$$v(x, y, z, t) = v_0(x, y, t) + z\psi_y(x, y, t) \tag{1c}$$

$$w_p(x, y, t) = w_C(t) + (x - x_C)\psi_C(t) + w(x, y, t) \tag{1d}$$

where $u_0$ and $v_0$ are midplane elastic deflections in the $x$ and $y$ directions, respectively, $\psi_x$ and $\psi_y$ are angular displacements of a line normal to the nominal plane of the plate due to elasticity, and $w$ is the elastic part of the transverse displacement.

Because the wing is attached to a fuselage that is assumed to be rigid, $w = 0$, $\psi_x = 0$, and $\psi_y = 0$ along $y = 0$. These are the only geometric boundary conditions of the problem.

## III. Extended Hamilton's Principle

The dynamical problem can be formulated by means of the extended Hamilton's principle, which can be written in the form[7]

$$\int_{t_1}^{t_2} (\delta T - \delta V + \overline{\delta W}_{nc})\, dt = 0$$

$$\delta w_C = \delta\psi_C = \delta w = \delta\psi_x = \delta\psi_y = 0 \quad \text{at} \quad t = t_1, t_2 \tag{2}$$

where $T$ is the kinetic energy, $V$ is the potential energy, and $\overline{\delta W}_{nc}$ is the virtual work performed by the nonconservative forces.

The kinetic energy arises from two sources, the motions of the fuselage and of the wing, and has the expression

$$\begin{aligned} T = T_f + T_w &= \frac{1}{2}\int [\dot{w}_C + (x - x_C)\dot{\psi}_C]^2\, dm_f \\ &+ \frac{1}{2}\int_0^s \int_{LE}^{TE} m\dot{w}_p^2\, dx\, dy \\ &= \frac{1}{2}(M_C\dot{w}_C^2 + I_C\dot{\psi}_C^2) + \dot{w}_C\int_0^s\int_{LE}^{TE} m\dot{w}\, dx\, dy \\ &+ \dot{\psi}_C\int_0^s\int_{LE}^{TE} m(x - x_C)\dot{w}\, dx\, dy + \frac{1}{2}\int_0^s\int_{LE}^{TE} m\dot{w}^2\, dx\, dy \end{aligned} \tag{3}$$

where $m_f$ is the mass of the fuselage, $m$ the mass per unit area of wing, $M_C$ the total mass of the system, and $I_C$ the pitch mass moment of inertia of the system about the mass center $C$. Moreover, $s$ denotes the wingspan, TE = TE($y$) the trailing edge, and LE = LE($y$) the leading edge.

The potential energy is assumed to be due entirely to the strain energy. In view of the layup symmetry, it is reasonable to assume that $u_0$ and $v_0$ are zero, so that the strain-displacement relations assume the simple form

$$\varepsilon_x = z\psi_{x,x} \tag{4a}$$

$$\varepsilon_y = z\psi_{y,y} \tag{4b}$$

$$\varepsilon_z = 0 \tag{4c}$$

$$\gamma_{yz} = \psi_y + w_{,y} \tag{4d}$$

$$\gamma_{xz} = \psi_x + w_{,x} \tag{4e}$$

$$\gamma_{xy} = z(\psi_{x,y} + \psi_{y,x}) \tag{4f}$$

where the shear strains are recognized as engineering shear strains. Moreover, the symbols ,$x$ and ,$y$ in the subscripts denote derivatives with respect to $x$ and $y$, respectively.

For the $j$th generally orthotropic layer with principal axes 1 and 2, the constitutive equations take the form

$$\begin{bmatrix} \sigma_1 \\ \sigma_2 \\ \tau_{23} \\ \tau_{13} \\ \tau_{12} \end{bmatrix}^j = [Q]^j \begin{bmatrix} \varepsilon_1 \\ \varepsilon_2 \\ \gamma_{23} \\ \gamma_{13} \\ \gamma_{12} \end{bmatrix}^j \tag{5}$$

The elements of $[Q]^j$ are related to material properties of the $j$th layer by

$$Q_{11}^j = \frac{E_1^j}{1 - \nu_{12}^j\nu_{21}^j} \tag{6a}$$

$$Q_{12}^j = \frac{\nu_{12}^j E_2^j}{1 - \nu_{12}^j\nu_{21}^j} \tag{6b}$$

$$Q_{22}^j = \frac{E_2^j}{1 - \nu_{12}^j\nu_{21}^j} \tag{6c}$$

$$Q_{44}^j = G_{23}^j \tag{6d}$$

$$Q_{55}^j = G_{13}^j \tag{6e}$$

$$Q_{66}^j = G_{12}^j \tag{6f}$$

where $E_i$, $G_{im}$, and $\nu_{im}$ are Young's moduli, shear moduli, and Poisson's ratios, respectively. The stress, engineering strain, and constitutive relationships for the $j$th layer can be written as follows:

$$\sigma_j' = [T_j]^{-1}\sigma_j'' \tag{7a}$$

$$\varepsilon_j' = [T_j]^{-1}\varepsilon_j'' \tag{7b}$$

$$\sigma_j' = [\bar{Q}_j]\varepsilon_j' \tag{7c}$$

where

$$[T_j] = \begin{bmatrix} \cos^2\theta_j & \sin^2\theta_j & 0 & 0 & \sin 2\theta_j \\ \sin^2\theta_j & \cos^2\theta_j & 0 & 0 & -\sin 2\theta_j \\ 0 & 0 & \cos\theta_j & -\sin\theta_j & 0 \\ 0 & 0 & \sin\theta_j & \cos\theta_j & 0 \\ -\frac{1}{2}\sin 2\theta_j & \frac{1}{2}\sin 2\theta_j & 0 & 0 & \cos 2\theta_j \end{bmatrix} \tag{8a}$$

$$[\bar{Q}_j] = [T_j]^{-1}[Q_j][T_j]^{-T} \tag{8b}$$

$$\sigma_j' = [\sigma_x \quad \sigma_y \quad \tau_{yz} \quad \tau_{xz} \quad \tau_{xy}]^T \tag{8c}$$

$$\sigma_j'' = [\sigma_1 \quad \sigma_2 \quad \tau_{23} \quad \tau_{13} \quad \tau_{12}]^T \tag{8d}$$

$$\varepsilon_j' = [\varepsilon_x \quad \varepsilon_y \quad (\gamma_{yz}/2) \quad (\gamma_{xy}/2) \quad (\gamma_{xy}/2)] \tag{8e}$$

$$\varepsilon_j'' = [\varepsilon_1 \quad \varepsilon_2 \quad (\gamma_{23}/2) \quad (\gamma_{13}/2) \quad (\gamma_{12}/2)] \tag{8f}$$

in which the conversion to engineering strain was taken into account. The angle $\theta_j$ is from the plate axis $x$ to the material axis $(1)_j$.

Next, we propose to derive the laminate strain energy. The laminate consists of $2k$ symmetrically stacked layers of variable thickness. Each layer height $t_j$ is a continuous function of $x$ and $y$ (Fig. 2). The strain energy density for a single layer $j$, or its counterpart below the midplane is

$$\hat{V}_j = \frac{1}{2}\int_{t_{j-1}}^{t_j} \sum_{i=1}^{5} \sigma_i^j \varepsilon_i^j \, dz \tag{9}$$

where $i = x, y, yz, xz, xy$. Summation over all of the layers and integration over the domain of the plate leads to the total strain energy

$$V = \frac{1}{2}\int_0^s \int_{\text{LE}}^{\text{TE}} \left[ \sum_{j=-k}^{k} \left( \int_{t_{j-1}}^{t_j} \sum_{i=1}^{5} \sigma_i^j \varepsilon_i^j \, dz \right) \right] dx \, dy \tag{10}$$

Substituting the strain-displacement relations [Eqs. (4)], and the constitutive relations [Eq. (7c)], into Eq. (10) and integrating over the layer thicknesses, we obtain the total strain energy expression

$$\begin{aligned} V = \frac{1}{2}\int_0^s \int_{\text{LE}}^{\text{TE}} \sum_{j=-k}^{k} \Big\{ & \frac{1}{3}(t_j^3 - t_{j-1}^3)[\psi_{x,x}^2 \bar{Q}_{11}^j + \psi_{y,y}^2 \bar{Q}_{22}^j \\ & + (\psi_{x,y} + \psi_{y,x})^2 \bar{Q}_{66}^j + 2\psi_{x,x}\psi_{y,y}\bar{Q}_{12}^j \\ & + 2\psi_{x,x}(\psi_{x,y} + \psi_{y,x})\bar{Q}_{16}^j + 2\psi_{y,y}(\psi_{x,y} + \psi_{y,x})\bar{Q}_{26}^j] \\ & + (t_j - t_{j-1})[(\psi_x + w_{,x})^2 \bar{Q}_{55}^j + (\psi_y + w_{,y})^2 \bar{Q}_{44}^j \\ & + 2(\psi_x + w_{,x})(\psi_y + w_{,y})\bar{Q}_{45}^j] \Big\} \, dx \, dy \end{aligned} \tag{11}$$

It must be recognized here that $t_j = t_j(x, y)$. The summation can be eliminated from the strain energy expression by considering the total laminate extensional and bending stiffness coefficients $A_{ab}$ and $D_{ab}$ defined as

$$\begin{aligned} A_{ab} &= \sum_{j=-k}^{k} (t_j - t_{j-1})\bar{Q}_{ab}^j \\ D_{ab} &= \frac{1}{3}\sum_{j=-k}^{k} (t_j^3 - t_{j-1}^3)\bar{Q}_{ab}^j \end{aligned} \tag{12}$$

and we observe that, because the thickness of the various layers is variable, $A_{ab} = A_{ab}(x, y)$ and $D_{ab} = D_{ab}(x, y)$. Using Eqs. (12), the total laminate strain energy can now be expressed in the compact form

$$V = \frac{1}{2}\int_0^s \int_{\text{LE}}^{\text{TE}} (\psi_D^T D \psi_D + \psi_A^T A \psi_A) \, dx \, dy \tag{13}$$

where

$$\psi_D = \begin{bmatrix} \psi_{x,x} \\ \psi_{y,y} \\ \psi_{x,y} + \psi_{y,x} \end{bmatrix} \tag{14a}$$

$$\psi_A = \begin{bmatrix} \psi_y + w_{,y} \\ \psi_x + w_{,x} \end{bmatrix} \tag{14b}$$

$$D = \begin{bmatrix} D_{11} & D_{12} & D_{16} \\ D_{12} & D_{22} & D_{26} \\ D_{16} & D_{26} & D_{66} \end{bmatrix} \tag{14c}$$

$$A = \begin{bmatrix} A_{44} & A_{45} \\ A_{45} & A_{55} \end{bmatrix} \tag{14d}$$

It remains to derive an expression for $\overline{\delta W}_{\text{nc}}$. Under consideration is a wing in the form of a trapezoidal planform, and in particular one characterized by low AR and/or forward-swept configuration. The most important speed regime for such a wing is undoubtedly supersonic. The main reason for including the aerodynamics is to demonstrate the usefulness of the structural model. A complete investigation of a wing would require appropriate aerodynamic theories for subsonic, transonic, supersonic, and perhaps hypersonic speed regimes. The usefulness of this model can be demonstrated with supersonic aerodynamics, chosen for relevancy and for relative ease of application. For large Mach numbers, $M^2 >> 1$, there is a weak memory effect, in addition to weak three-dimensional effects. This opens up the prospect of a point-function relation between the pressure difference $p_u - p_l$ and the displacement $w$ of the wing, which makes it both convenient and useful. The structural model is suitable for wings of any AR. Whereas piston theory is used to study this model, it must be noted that it is not as suitable for very low ARs as more sophisticated theories. This point function property permits the definition of an explicit aerodynamic operator operating on the vertical displacement of the wing, so that the force density can be written in the form[8]

$$A_{11}w_p = -C(x)\left(\frac{\partial}{\partial x} + \frac{1}{U}\frac{\partial}{\partial t}\right) w_p \tag{15}$$

where

$$C(x) = \frac{4q}{M}\left(1 + \frac{\gamma + 1}{2} M \frac{dt_N}{dx}\right) \tag{16}$$

in which $M$ is the Mach number, $q$ the dynamic pressure, $t_N$ the wing half-thickness, $U$ the freestream airspeed, and $\gamma$ the ratio of specific heats.

The nonconservative virtual work is due to the aerodynamic forces and can be obtained by multiplying the distributed force [Eq. (15)], by the corresponding virtual displacement and integrating over the domain of the wing. Then, using Eq. (1d), we obtain

$$\begin{aligned} \overline{\delta W}_{\text{nc}} \int_0^s \int_{\text{LE}}^{\text{TE}} A_{11} w_p \delta w_p \, dx \, dy &= W_C \delta w_C \\ + \Psi_C \delta \psi_C + \int_0^s \int_{\text{LE}}^{\text{TE}} \hat{W} \delta w \, dx \, dy & \end{aligned} \tag{17}$$

where

$$W_C = -\int_0^s \int_{LE}^{TE} C(x) \left\{ \psi_C + w_{,x} + \frac{1}{U} [\dot{w}_C + (x - x_C)\dot{\psi}_C + \dot{w}] \right\} dx\, dy \tag{18a}$$

is a resultant aerodynamic force

$$\Psi_C = -\int_0^s \int_{LE}^{TE} C(x) \left\{ \psi_C + w_{,x} + \frac{1}{U} \times [\dot{w}_C + (x - x_C)\dot{\psi}_C + \dot{w}] \right\} (x - x_C)\, dx\, dy \tag{18b}$$

is a resultant aerodynamic moment about an axis parallel to $y$ and passing through $C$ and

$$\hat{W} = -C(x)\{\psi_C + w_{,x} + (1/U)[\dot{w}_C + (x - x_C)\dot{\psi}_C + \dot{w}]\} \tag{18c}$$

is an aerodynamic force density.

## IV. Eigenvalue Problem

Inserting Eqs. (3), (13), and (16) into the extended Hamilton's principle and following the usual steps,[7] we can obtain the boundary-value problem for the system. The boundary-value problem consists of two ordinary differential equations (ODEs) for $w_0(t)$ and $\psi_C(t)$ and three partial differential equations (PDEs) for $w(x, y, t)$, $\psi_x(x, y, t)$, and $\psi_y(x, y, t)$, together with appropriate boundary conditions.

The differential eigenvalue problem can be obtained from the boundary-value problem by assuming that the displacements vary exponentially with time. The state of the art does not permit a closed-form solution of the differential eigenvalue problem, so that one must be content with an approximate solution, which amounts to spatial discretization of the problem through a series expansion. As a result, the original differential eigenvalue problem is replaced by an algebraic eigenvalue problem. It turns out that, in deriving the algebraic eigenvalue problem, it is more efficient to carry out the spatial discretization directly in the extended Hamilton's principle [Eq. (2)]. To this end, we assume a solution of the form

$$w_C(t) = q_1(t) \tag{19a}$$

$$\psi_C(t) = q_2(t) \tag{19b}$$

$$w(x, y, t) = \sum_{i=3}^{n+2} \phi_i(x, y) q_i(t) \tag{19c}$$

$$\psi_x(x, y, t) = \sum_{i=n+3}^{2n+2} \phi_i(x, y) q_i(t) \tag{19d}$$

$$\psi_y(x, y, t) = \sum_{i=2n+3}^{3n+2} \phi_i(x, y) q_i(t) \tag{19e}$$

where $\phi_i$ are space-dependent trial functions and $q_i$ are time-dependent generalized coordinates. Inserting Eqs. (19) into Eq. (3) and omitting the integral limits for simplicity of notation, we can write the kinetic energy in the discretized form

$$T = \frac{1}{2}(M_C \dot{w}_C^2 + I_C \dot{\psi}_C^2) + \dot{w}_C \int\int m\dot{w}\, dx\, dy + \dot{\psi}_C \int\int m(x - x_C)\dot{w}\, dx\, dy + \frac{1}{2}\int\int m\dot{w}^2\, dx\, dy = \frac{1}{2}\dot{\boldsymbol{q}}^T M \dot{\boldsymbol{q}} \tag{20}$$

where $\boldsymbol{q}$ is a $3n$ vector of displacement amplitudes and $M$ is the symmetric mass matrix having the components

$$M_{11} = M_C \tag{21a}$$

$$M_{12} = 0 \tag{21b}$$

$$M_{1j} = \int\int m\phi_j\, dx\, dy, \qquad 3 \le j \le n + 2 \tag{21c}$$

$$M_{1j} = 0, \qquad j > n + 2 \tag{21d}$$

$$M_{21} = 0 \tag{21e}$$

$$M_{22} = I_C \tag{21f}$$

$$M_{2j} = \int\int m(x - x_C)\phi_j\, dx\, dy, \qquad 3 \le j \le n + 2 \tag{21g}$$

$$M_{2j} = 0, \qquad j > n + 2 \tag{21h}$$

$$M_{ij} = \int\int m\phi_i\phi_j\, dx\, dy, \qquad 3 \le i, \quad j \le n + 2 \tag{21i}$$

$$M_{ij} = 0, \qquad i, j > n + 2 \tag{21j}$$

Moreover, introducing Eqs. (19c–19e) into Eq. (13), and considering Eqs. (14), we obtain the discretized potential energy

$$V = \frac{1}{2}\int\int (\psi_D^T \psi_D + \psi_A^T A \psi_A)\, dx\, dy = \frac{1}{2}\boldsymbol{q}^T K \boldsymbol{q} \tag{22}$$

where $K$ is the symmetric stiffness matrix having the entries

$$K_{ij} = 0, \qquad i = 1, 2 \quad \text{and} \quad 1 \le j \le 3n + 2 \tag{23a}$$

$$K_{ij} = \int\int [\phi_{i,x}\phi_{j,x}A_{55} + (\phi_{i,y}\phi_{j,x} + \phi_{i,x}\phi_{j,y})A_{45} + \phi_{i,y}\phi_{j,y}A_{44}]\, dx\, dy, \qquad 3 \le i, \quad j \le n + 2 \tag{23b}$$

$$K_{ij} = \int\int (\phi_{i,x}\phi_j A_{55} + \phi_{i,y}\phi_j A_{45})\, dx\, dy \qquad 3 \le i \le n + 2, \quad n + 3 \le j \le 2n + 2 \tag{23c}$$

$$K_{ij} = \int\int (\phi_{i,x}\phi_j A_{45} + \phi_{i,y}\phi_j A_{44})\, dx\, dy \qquad 3 \le i \le n + 2, \quad 2n + 3 \le j \le 3n + 2 \tag{23d}$$

$$K_{ij} = \int\int [\phi_i\phi_j A_{55} + \phi_{i,x}\phi_{j,x}D_{11} + \phi_{i,y}\phi_{j,y}D_{66} + (\phi_{i,y}\phi_{j,x} + \phi_{i,x}\phi_{j,y})D_{16}]\, dx\, dy \qquad n + 3 \le i, \quad j \le 2n + 2 \tag{23e}$$

$$K_{ij} = \int\int (\phi_i\phi_j A_{45} + \phi_{i,x}\phi_{j,x}D_{16} + \phi_{i,y}\phi_{j,x}D_{66} + \phi_{i,x}\phi_{j,y}D_{12} + \phi_{i,y}\phi_{j,y}D_{26})\, dx\, dy \qquad n + 3 \le i \le 2n + 2, \quad 2n + 3 \le j \le 3n + 2 \tag{23f}$$

$$K_{ij} = \int\int [\phi_i\phi_j A_{44} + \phi_{i,x}\phi_{j,x}D_{66} + \phi_{i,y}\phi_{j,y}D_{22} + (\phi_{i,y}\phi_{j,x} + \phi_{i,x}\phi_{j,y})D_{26}]\, dx\, dy \qquad 2n + 3 \le i, \quad j \le 3n + 2 \tag{23g}$$

Finally, inserting Eqs. (19c–19e) into Eq. (17) and considering Eqs. (18), we can write the discretized virtual work due to aerodynamic forces in the form

$$\overline{\delta W}_{nc} = W_C \delta w_C + \Psi_C \delta \psi_C + \int\int \hat{W} \delta w \, dx \, dy = -\delta \boldsymbol{q}^T \left( K_A \boldsymbol{q} + \frac{1}{U} H \dot{\boldsymbol{q}} \right) \tag{24}$$

where the entries of the nonsymmetric matrix $K_A$ are

$$K_{A1j} = 0, \quad j = 1, 2, \ldots, n+2 \tag{25a}$$

$$K_{A21} = \int\int C \, dx \, dy \tag{25b}$$

$$K_{A22} = \int\int C(x - x_C) \, dx \, dy \tag{25c}$$

$$K_{A2j} = \int\int C\phi_j \, dx \, dy, \quad 3 \le j \le n+2 \tag{25d}$$

$$K_{Ai1} = \int\int C\phi_{i,x} \, dx \, dy, \quad 3 \le i \le n+2 \tag{25e}$$

$$K_{Ai2} = \int\int C(x - x_C)\phi_{i,x} \, dx \, dy, \quad 3 \le i \le n+2 \tag{25f}$$

$$K_{Aij} = \int\int C\phi_{i,x}\phi_j \, dx \, dy, \quad 3 \le i, \quad j \le n+2 \tag{25g}$$

$$K_{Aij} = 0, \quad 1 \le i \le n+2, \quad j > n+2 \tag{25h}$$

$$K_{Aij} = 0, \quad i > n+2 \tag{25i}$$

and those of the symmetric matrix $H$ are

$$H_{11} = \int\int C \, dx \, dy \tag{26a}$$

$$H_{12} = \int\int C(x - x_C) \, dx \, dy \tag{26b}$$

$$H_{1j} = \int\int C\phi_j \, dx \, dy, \quad 3 \le j \le n+2 \tag{26c}$$

$$H_{22} = \int\int C(x - x_C)^2 \, dx \, dy \tag{26d}$$

$$H_{2j} = \int\int C(x - x_C)\phi_j \, dx \, dy, \quad 3 \le j \le n+2 \tag{26e}$$

$$H_{ij} = \int\int C\phi_i\phi_j \, dx \, dy, \quad 3 \le i, \quad j \le n+2 \tag{26f}$$

$$H_{ij} = 0, \quad 1 \le i \le n+2, \quad j > n+2 \tag{26g}$$

$$H_{ij} = 0, \quad i > n+2 \tag{26h}$$

Introducing Eqs. (20), (22), and (24) into Eq. (2), integrating the term involving $\delta\dot{\boldsymbol{q}}$ by parts with respect to time and invoking the arbitrariness of $\delta\boldsymbol{q}$, we obtain a set of simultaneous ODEs, which can be written in the compact form:

$$M\ddot{\boldsymbol{q}} + (1/U)H\dot{\boldsymbol{q}} + (K + K_A)\boldsymbol{q} = \boldsymbol{0} \tag{27}$$

Then, letting

$$\boldsymbol{q}(t) = e^{\lambda t}\boldsymbol{a} \tag{28}$$

we obtain the desired algebraic eigenvalue problem

$$[\lambda^2 M + (\lambda/U)H + K + K_A]\boldsymbol{a} = \boldsymbol{0} \tag{29}$$

and we note that the problem is non-self-adjoint due to the presence of the aerodynamic matrices $H$ and $K_A$.

The solution of the eigenvalue problem [Eq. (29)] requires that it be cast in state form. To this end, we introduce the state vector $\boldsymbol{x} = [\boldsymbol{a}^T \ \lambda\boldsymbol{a}^T]^T$. Then, adjoining the identity $\lambda\boldsymbol{a} = \lambda\boldsymbol{a}$, Eq. (29) can be rewritten in the state form

$$A\boldsymbol{x} = \lambda B\boldsymbol{x} \tag{30}$$

where

$$A = \begin{bmatrix} 0 & I \\ -(K + K_A) & -H/U \end{bmatrix} \tag{31a}$$

$$B = \begin{bmatrix} I & 0 \\ 0 & M \end{bmatrix} \tag{31b}$$

Because the matrix $B$ is singular, some of the eigenvalues are infinite. Numerical solutions for this type of eigenvalue problem can be obtained by an algorithm described in Ref. 9.

## V. Approximate Solutions in Terms of Quasi-Comparison Functions

In Sec. IV, a discretized model for the system is derived by assuming an approximate solution in the form of a linear combination of trial functions. The accuracy of the approximate solution and the computational time depend on the nature of the trial functions. To examine the nature of the trial functions, a brief discussion of the various classes of functions should prove beneficial.

Exact, closed-form solutions of differential eigenvalue problems represent the class of eigenfunctions. Clearly, they satisfy both the differential equations and all the boundary conditions of the problem. In most practical problems, closed-form solutions do not exist. They certainly do not exist in the problem at hand. Approximate solutions generally fail to satisfy the differential equations. Functions satisfying certain differentiability conditions and all the boundary conditions, but not necessarily the differential equations, are called comparison functions.[7] In many problems, including that under consideration, comparison functions are difficult to generate. In the case of self-adjoint systems, it is often advantageous to formulate the eigenvalue problem by a variational approach, which amounts to rendering Rayleigh's quotient stationary. In this case, the trial functions need to satisfy reduced differentiability conditions and the geometric boundary conditions alone. Such functions are known as admissible functions,[7] or more popularly as shape functions. It has been demonstrated in Ref. 6 that on occasions, solutions in terms of admissible functions converge very slowly. To improve convergence, a new class of functions was created in Ref. 10, namely, the class of quasi-comparison functions. The quasi-comparison functions are linear combinations of admissible functions capable of satisfying all the boundary conditions of the problem. Quasi-comparison functions can be generated by combining several families of admissible functions chosen so as to permit the satisfaction of the natural boundary conditions. It turns out that solutions in terms of quasi-comparison functions tend to satisfy not only the natural boundary conditions, but also the differential equations much more accurately than solutions in terms of mere admissible functions. In fact, solutions in terms of quasi-comparison functions can at times be more accurate than solutions in terms of comparison functions, because combinations of functions from several families with different characteristics permit better approximations of the solution throughout the interior of the domain than combinations of functions from a single family.[6,10] In Refs. 11 and 12, it was demonstrated that solutions in terms of quasi-comparison functions exhibit the same superior convergence characteristics in the case of non-self-adjoint systems as well. In this regard, it must be pointed out that the system considered here falls in the general class of non-self-adjoint systems.

In view of the previous discussion, the trial functions in Eqs. (19c–19e) are chosen from the class of quasi-comparison functions. These functions must depend on both $x$ and $y$ and are assumed to have the form of products of chordwise functions $X_{k_f}(x)$ and spanwise functions $Y_{l_f}(y)$. The eigenvalue problem is defined in terms of trial functions $\phi_i$ and $\phi_j$ ($i, j = 1, 2, 3, \ldots, 3n + 2$), where $n$ is the number of trial functions for each of the three displacements $w$, $\psi_x$, and $\psi_y$. There are additionally two rigid-body modes, namely, $\phi_1 = 1$ and $\phi_2 = 1$. Let the same set of trial functions be used for each of the displacements $w$, $\psi_x$, and $\psi_y$. The undetermined coefficients, of course, are not the same. Then, for $i = 3, 4, 5, \ldots, 3n + 2$

$$\phi_f(x, y) = X_{k_f}(x)Y_{l_f}(y), \qquad 1 \le f \le n \tag{32a}$$

where

$$f = i - 2 - n \cdot \mathrm{INT}[(i - 2)/n] \tag{32b}$$

Similarly, for the companion set of trial functions

$$\phi_g = X_{k_g}(x)Y_{l_g}(y), \qquad 1 \le g \le n \tag{32c}$$

in which

$$g = j - 2 - n \cdot \mathrm{INT}[(j - 2)/n] \tag{32d}$$

where INT( ) implies truncation to the corresponding integer value.

The functions $X_{k_f}$ and $Y_{l_f}$ are each chosen from two different families. The indices $k_f$ and $l_f$ determine the order of combination of functions $X_{k_f}$ and $Y_{l_f}$ into $\phi_f$, and hence, they depend on $f$, which in turn depends on $i$ according to Eq. (32b). Because the interest is in low AR wings, the dependence of $k_f$ and $l_f$ on $f$ is such that the spanwise and chordwise functions are about equal in number or

$$l_f = f - \tfrac{1}{2}(d^2 - d), \quad f = 1, 2, 3, \ldots, (n/2) \tag{33a}$$

$$l_f = \tfrac{1}{2}(2f - n - d^2 + d), \quad f = (n/2) + 1, (n/2) + 2, \ldots, n \tag{33b}$$

$$k_f = 1 - d - l_f, \quad f = 1, 2, 3, \ldots, n \tag{33c}$$

where

$$d = \mathrm{NINT}\sqrt{2f}, \quad f = 1, 2, 3, \ldots, (n/2) \tag{34a}$$

$$d = \mathrm{NINT}\sqrt{2f - n}, \quad f = (n/2) + 1, (n/2) + 2, \ldots, n \tag{34b}$$

and NINT( ) implies rounding to the nearest integer value. It is assumed in Eqs. (33) and (34) that $n$ is an even integer. Equations (33) and (34) define the selection order of spanwise and chordwise functions for a given family of admissible functions used to generate the quasi-comparison functions of Eqs. (32). Table 1 clarifies this selection order.

The chordwise functions $X_{k_f}(x)$ are segments of a sine function with an appropriate number of zero crossings. Accounting for leading- and trailing-edge sweep $\eta_L$ and $\eta_T$, and for the resulting variable limits on $x$, $X_{k_f}$ actually becomes a function of both $x$ and $y$. The first family of chordwise functions are chosen as

$$X_{k_f}(x, y) = \sin\left\{\frac{3\pi}{4} + \pi\left(k_f - \frac{3}{2}\right) \times \left[\frac{x - y\tan\eta_L}{r - y(\tan\eta_L - \tan\eta_T)}\right]\right\}, \qquad \mathrm{LE} \le x \le \mathrm{TE} \tag{35}$$

**Table 1 Function selection order**

| Chordwise function count, $k_f(k_g)$ | Spanwise function count $l_f(l_g)$ | | | | | | |
|---|---|---|---|---|---|---|---|
| | 1 | 2 | 3 | 4 | 5 | 6 | 7 |
| 1 | 1 | 3 | 6 | 10 | 15 | 21 | 28 |
| 2 | 2 | 5 | 9 | 14 | 20 | 27 | |
| 3 | 4 | 8 | 13 | 19 | 26 | | |
| 4 | 7 | 12 | 18 | 25 | | | |
| 5 | 11 | 17 | 24 | | | | |
| 6 | 16 | 23 | | | | | |
| 7 | 22 | | | | | | |

The spanwise functions $Y_{l_f}(y)$ are also appropriate segments of a sine function with an appropriate number of zero crossings, or

$$Y_{l_f}(y) = \frac{y}{s}\sin\left[\frac{(2l_f - 1)\pi}{2s}y\right], \qquad 0 \le y \le s \tag{36}$$

The second family of functions $X_{k_f}$ consists of terms from a power series, except that the functions alternate direction between the leading and trailing edge. The sweep of the leading- and trailing-edges $\eta_L$ and $\eta_T$ requires shifting and scaling as before, resulting in

$$X_{k_f}(x, y) = \langle\{r[1 + (-1)^{k_f}] - (-1)^{k_f}x + [1 + (-1)^{k_f}](\tan\eta_T - \tan\eta_L)y\}/2[r + (\tan\eta_T - \tan\eta_L)y]\rangle^{\mathrm{INT}[(k_f+3)/2]}, \qquad \mathrm{LE} \le x \le \mathrm{TE} \tag{37}$$

where INT( ) implies truncation to the corresponding integer value. Equation (37) appears complicated, but it merely represents a power series shifted and scaled, and alternating in direction so as to accommodate the swept boundaries. The second family of spanwise functions is simply

$$Y_{l_f}(y) = (y/s)^{\mathrm{INT}[(l_f+3)/2]}, \qquad 0 \le y \le s \tag{38}$$

The algebraic eigenvalue problem is assembled for $f$ and $g$ from 1 to $n$. The entries of the matrices $M$, $K$, $K_A$, and $H$ are given by Eqs. (21), (23), (25), and (26), respectively. The complete set of two-dimensional quasi-comparison functions is expressed in terms of $f$ through $l_f$ and $k_f$ as follows:

$$\phi_f = \frac{y}{s}\sin ay, \quad f = 3, 4, \ldots, \frac{n + 2}{2}, \quad k_f = 1 \tag{39a}$$

$$\phi_f = \frac{xy}{rs}\sin ay, \quad f = 3, 4, \ldots, \frac{n + 2}{2}, \quad k_f = 2 \tag{39b}$$

$$\phi_f = \frac{y}{s}\sin ay \sin\frac{b + cx + dy}{r + ey} \quad f = 3, 4, \ldots, \frac{n + 2}{2}, \quad k_f \ge 3 \tag{39c}$$

$$\phi_f = \left(\frac{y}{s}\right)^N, \quad f = \frac{n + 4}{2}, \ldots, n, \quad k_f = 1 \tag{40a}$$

$$\phi_f = \frac{x}{r}\left(\frac{y}{s}\right)^N, \quad f = \frac{n + 4}{2}, \ldots, n, \quad k_f = 2 \tag{40b}$$

$$\phi_f = My^N\left[\frac{1}{2}(1 - Q) + Q\frac{x + yp}{r + ye}\right]^s \quad f = \frac{n + 4}{2}, \ldots, n, \quad k_f \ge 3 \tag{40c}$$

where

$$b = \frac{3r\pi}{4} \tag{41a}$$

$$e = \tan \eta_T - \tan \eta_L \tag{41b}$$

$$p = -\tan \eta_L \tag{41c}$$

$$a = \frac{(2l_f - 1)\pi}{2s} \tag{41d}$$

$$c = \pi\left(k_f - \frac{3}{2}\right) \tag{41e}$$

$$d = \pi\left[\frac{3}{4}e + \left(k_f - \frac{3}{2}\right)p\right] \tag{41f}$$

$$M = \left(\frac{1}{s}\right)^N \tag{41g}$$

$$N = \frac{l_f + 3}{2} \tag{41h}$$

$$Q = -(-1)^{k_f} \tag{41i}$$

$$s = \text{INT}\left(\frac{k_f + 1}{2}\right) \tag{41j}$$

Similar series can be written for $\phi_g$ by replacing $f$ by $g$ and $i$ by $j$. The simpler forms for $\phi_f$ when $k_f = 1, 2$ are due to the simple form of the rigid chordwise shape functions corresponding to the first two terms in $X_{k_f}(x)$, as mentioned previously. An example of the series $\phi_f(x, y)$ for $n = 6$ should prove helpful. The six terms consist of three terms from each of the two families, or

$$\phi_1 = \frac{y}{s}\sin\frac{\pi}{2s}y \tag{42a}$$

$$\phi_2 = \frac{xy}{rs}\sin\frac{\pi}{2s}y \tag{42b}$$

$$\phi_3 = \frac{y}{s}\sin\frac{3\pi}{2s}y \tag{42c}$$

$$\phi_4 = \left(\frac{y}{s}\right)^2 \tag{42d}$$

$$\phi_5 = \frac{x}{r}\left(\frac{y}{s}\right)^2 \tag{42e}$$

$$\phi_6 = \left(\frac{y}{s}\right)^{2.5} \tag{42f}$$

## VI. Numerical Results

In presenting numerical results, it is useful to define several dimensionless quantities. The frequency can be nondimensionalized as follows:

$$\Omega = \omega A\left[\frac{\rho_{\text{ref}}}{E_{\text{ref}}t_{\text{ref}}^2}\right]^{1/2} \tag{43}$$

Similarly, a speed parameter can be defined, yielding the dimensionless dynamic pressure

$$\lambda_a = \frac{2qA^2}{E_{\text{ref}}t_{\text{ref}}^4} = \frac{\rho_{\text{air}}U^2A^2}{E_{\text{ref}}t_{\text{ref}}^4} \tag{44}$$

The quantities $(\ )_{\text{ref}}$ are reference values. The quantities $E_{\text{ref}}$ and $\rho_{\text{ref}}$ represent $E_2$ and $\rho$ for the main structural material, and $t_{\text{ref}}$ is the total thickness at the wing root and leading-edge intersection. Other dimensionless parameters are the taper ratio TR and the aspect ratio AR. Extensive vibration and flutter results have been generated with this model. The intent here is to develop and present the formulation, so that the presented results are merely a summary of those obtained.

### A. Convergence and Accuracy

The convergence of the free-vibration eigenvalues of an anisotropic low AR wing, designated as AN1 in Table 2, is considered in Fig. 3. The material properties are as in Table 3. The convergence rate of the first five nonzero eigenvalues is depicted as the frequency parameter $\Omega$ vs the number of terms in the approximating series. The first two eigenvalues have zero value and correspond to rigid-body modes, which converge immediately; they are not shown in Fig. 3. It should be pointed out here that a linear combination of admissible functions must possess a minimum number of terms before it qualifies as a quasi-comparison function. The number must be such as to permit satisfaction of all natural boundary conditions. As soon as this number of terms has been reached, convergence of the computed eigenvalues to the actual ones is relatively rapid, as can be concluded from Fig. 3.

The two flutter mechanisms of most concern are the bending-torsion mode and the body-freedom mode. The body-freedom flutter mode occurs instead of the divergence mode when the pitch DOF is introduced. Reasonably accurate representations of the pitch mode and the first two flexible modes, as well as fairly accurate representation of the third flexible mode, are required to capture these two mechanisms. The indications from Fig. 3 are that 20 terms are sufficient for this purpose, certainly for establishing a trend.

Convergence of the flutter dynamic pressure parameter for a forward-swept variant of AN1 is shown in Fig. 4. The flutter mechanism acting is body-freedom flutter. Reasonable convergence has been achieved with 20 terms.

Figure 5 shows three frequencies corresponding to an isotropic plate of AR 5; the computed values are compared with the exact values given in Table 11.4 of Ref. 13. The plate is $\frac{1}{2}$-in. steel, designated as PL1 in Table 2, and is fixed on a short side. The remaining three edges are free. The clamped condition is simulated with the present model by taking very large values for fuselage mass and pitch inertia. The results are quite acceptable. As expected from the discussion of quasicomparison functions, the approximations are poor for small numbers of terms, but begin to converge to the actual values quite rapidly when a certain critical number of terms is reached.

The accuracy of the flutter analysis is checked through a comparison with results obtained in Ref. 14 by Rossettos and Tong, which is one of the few works available on the flutter of a plate with free edges in the supersonic region. Their model consists of a single layer, constant thickness, square composite plate clamped at one edge and subjected to super-

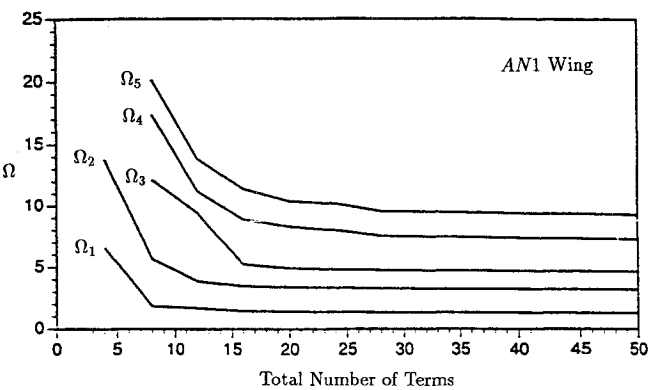


**Fig. 3 Frequency parameter convergence.**

**Table 2 Example wings**

| Designation: | AN1 | OR1 | IS1 | PL1 | PL2 |
|---|---|---|---|---|---|
| Layer materials | 1C/4GE | 1C/4GE | 1C/1A/1GE | 1S | 1R |
| Tailoring layer | 5 | 5 | 3 | — | — |
| Total wing area, in.$^2$ | 40,320 | 40,320 | 40,320 | 4204.8 | 20,000 |
| TR | 0.3333 | 0.3333 | 0.3333 | 1 | 1 |
| AR | 3 | 3 | 8 | 5 | 2 |
| Midchord sweepback, deg | 0 | 0 | −20.0 | 0 | 0 |
| Nonwing aircraft weight, lb | 18,000 | 18,000 | 18,000 | ∞ | ∞ |
| Nonwing aircraft pitch inertia, lb-in.-s$^2$ | 5.0E7 | 5.0E7 | 5.0E7 | ∞ | ∞ |
| Nonwing aircraft c.g. as percent root chord | 0.46 | −0.35 | −0.25 | — | — |
| Total fuel weight, lb | 1,200 | 1,200 | 1,200 | 0 | 0 |
| Total nonskin wing structural weight, lb | 1,000 | 1,000 | 1,000 | 0 | 0 |
| Thickness of the first layer | | | | | |
| LE, ROOT | 3.284 | 2.500 | 5.000 | 0.25 | 0.7122 |
| TE, ROOT | 0.682 | 2.500 | 5.000 | 0.25 | 0.7122 |
| LE, TIP | 1.006 | 1.000 | 2.000 | 0.25 | 0.7122 |
| Thickness of the second layer | | | | | |
| LE, ROOT | 0.0595 | 0.0500 | 0.210 | — | — |
| TE, ROOT | 0.0455 | 0.0500 | 0.210 | — | — |
| LE, TIP | 0.0405 | 0.0300 | 0.126 | — | — |
| Thickness of the third layer | | | | | |
| LE, ROOT | 0.0475 | 0.0500 | 0.0500 | — | — |
| TE, ROOT | 0.0595 | 0.0500 | 0.0500 | — | — |
| LE, TIP | 0.0350 | 0.0300 | 0.0300 | — | — |
| Thickness of the fourth layer | | | | | |
| LE, ROOT | 0.0440 | 0.0500 | — | — | — |
| TE, ROOT | 0.0300 | 0.0500 | — | — | — |
| LE, TIP | 0.0370 | 0.0300 | — | — | — |
| Thickness of the fifth layer | | | | | |
| LE, ROOT | 0.0649 | 0.0600 | — | — | — |
| TE, ROOT | 0.0581 | 0.0600 | — | — | — |
| LE, TIP | 0.0484 | 0.0360 | — | — | — |
| Layer orientation from midchord, deg AFT | −/−17/38 −52/0/− | −/−45/45 0/0/− | −/−/0 | — | 0 |

**Table 3 Material properties**

| | Low stiffness core, "C" | Aluminum, "A" | Steel, "S" | Graphite epoxy, "GE" |
|---|---|---|---|---|
| $E_1$, lb-in.$^2$ | 100 | 1.03E7 | 3.0E7 | 2.1E7 |
| $E_2$, lb-in.$^2$ | 100 | 1.03E7 | 3.0E7 | 1.7E6 |
| $\nu_{21}$ | 0.3 | 0.334 | 0.3 | 0.017 |
| $\nu_{12}$ | 0.3 | 0.334 | 0.3 | 0.210 |
| $G_{23}$, lb-in.$^2$ | 30 | 3.8E6 | 1.15E7 | 6.5E5 |
| $G_{13}$, lb-in.$^2$ | 30 | 3.8E6 | 1.15E7 | 6.5E5 |
| $G_{12}$, lb-in.$^2$ | 30 | 3.8E6 | 1.15E7 | 6.5E5 |
| $\rho$, lb-in.$^{-3}$ | 0.00116 | 0.098 | 0.283 | 0.054 |

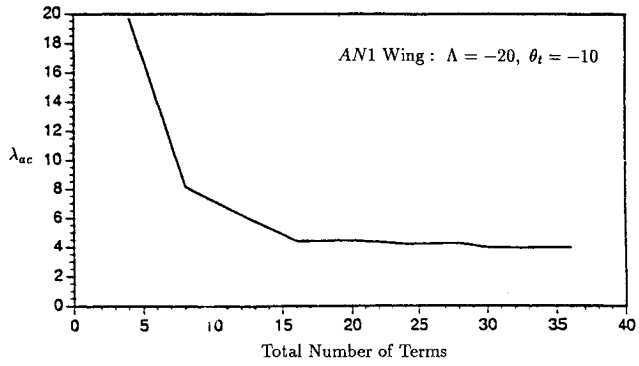


**Fig. 4 Convergence of the flutter dynamic pressure.**

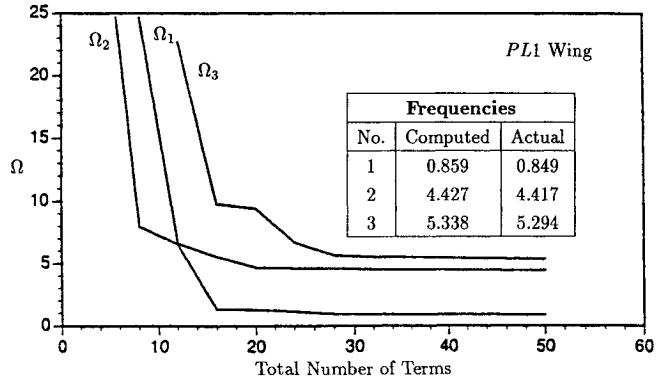


**Fig. 5 Frequency parameter convergence.**

sonic flow on the upper surface. The aerodynamics is based on a variant of the piston theory that converges to Eq. (15) for sufficiently high Mach numbers and with flow over both surfaces. Comparison is for a square composite plate, denoted by PL2 in Table 2, with a fiber orientation of 24 deg. The model derived here predicted on the average flutter speeds 6% higher than those of Ref. 14.

### B. Free Vibration Results

The interest in the free vibration case is mainly due to its relation to the flutter case. The two flutter mechanisms, body-freedom and bending-torsion, dictate that concentration is on

the pitch mode and the first two flexible modes, although the first few flexible modes above these will also have some influence. The convergence of the rigid-body modes, pitch and plunge, is not an issue.

For body-freedom flutter, the most critical parameter is geometrical. If the wing is not swept forward, or nearly so, then this flutter mechanism is not likely to arise. Work by a number of authors demonstrates a surprising influence of a tailoring layer swept just a few degrees off nominal. Body-freedom flutter can be eliminated, or pushed up to significantly higher speeds, if a percentage of the spanwise plies are reoriented 10-deg forward. Two factors are at work in this case and both are free-vibration matters. When an orthotropic layer for which $E_1 >> E_2$ is reoriented, bending begins to occur in the direction normal to $E_1$. The result is an effective rotation of the elastic axis in the direction opposite to the reorientation of the tailoring ply. The other factor at work is the necessary reduction of spanwise bending stiffness that must accompany the reorienting of plies away from the midchord. This second factor eventually overpowers the first, so that ply reorientations are most effective when they are small.

Figure 6 shows the frequency parameter of the first flexible mode varying with the sweep angle of a tailoring layer. The results for three wings are shown. An interesting phenomenon is observed in Fig. 6 for the low AR wing. This wing has its highest bending stiffness associated with a significantly aft-swept tailoring layer $\theta = 10$ deg. The implication is that tailoring plies might not be as effective for low AR wings. This trend, shown to be true in the next subsection, was not previously discovered due to inherent limitations of the one-dimensional models commonly used.

Much has been said about the benefits of using the anisotropy of a composite layup to tailor the response of a wing. Such discussion has been limited almost entirely to ply orientation. The dominant use of one-dimensional structural models has forced this limitation on the current investigation. One can easily suppose that distribution of the tailoring material in both the spanwise and chordwise directions might significantly affect the response. These trends are readily investigated with the current plate model. As ply distribution for the AN1 example wing is varied from full depth at the trailing edge to full depth at the leading edge, there is a change in frequency of the natural modes. The associated frequency parameters increase by 8, 6, and 3%, respectively, for the first three flexible modes. The bending-torsion separation increases by 5%. For a similar spanwise variation from wingtip concentration to wing root, frequencies again vary. In this case, the increases are 34, 14, and 12%, respectively, for the first three flexible modes. For bending-torsion separation, the change is slight at 2.5%. This reflects the increase in bending stiffness, which occurs when material is shifted near the wing root. Clearly, the two-dimensional nature of this material distribution has an effect on the free vibration outcome. It seems reasonable to expect that the flutter response will also be affected, allowing a refinement of the concept of tailoring with composites.

### C. Flutter Analysis Results

Two flutter mechanisms are of primary concern for a symmetric model of a wing with forward or aft sweep. The first is the classical bending-torsion flutter that can occur for a wing of any sweep when the frequencies of these two modes begin to coalesce as the airspeed increases, with one root becoming increasingly stable while the other root, after becoming more stable initially, tends to become unstable. The corresponding frequencies coalesce as the instability approaches. Complete coalescence does not occur when the fuselage is capable of rigid-body motions. The rigid-body pitch frequency assumes a nonzero value, which rises as the speed increases. Without a tailored layup, the pitch and bending modes would surely combine to cause body-freedom flutter before the bending-torsion coupling could arise. Recall that bending-torsion flutter is unlikely at any speed for a significant forward sweep angle. It is seen then that the same tailoring which eliminates body-freedom flutter by apparent aft sweeping of the elastic axis also makes bending-torsion flutter possible. A tradeoff is implied and caution must be exercised when contemplating a tailored composite design solution.

Next, the characteristics of body-freedom flutter are considered. For the orthotropic (OR1) example wing of Table 2 with $\Lambda = -30$ deg, the flutter mode will be body-freedom flutter, or divergence if clamped. The bending-torsion case occurs at a much higher speed or may not occur at all for a large forward sweep angle. The pitch mode is characteristically very lightly damped and tends to move toward instability as the bending mode moves away from the imaginary axis. The pitch and bending frequencies coalesce eventually with increasing dynamic pressure rather than separating, as would be the case for bending-torsion flutter.

Weisshaar et al.[1] have reported a trend in the ratio $\Omega_{\text{flutter}}/\Omega_{\text{fundamental}}$ for the two flutter mechanisms just presented. In a particular case in Ref. 1, the ratio is equal to 0.26 for a body-freedom flutter and to 3.40 for a bending-torsion flutter. The ratios for comparable cases in this work are 0.42 and 2.64, respectively.

The effect of tailoring plies, particularly on divergence or body-freedom flutter has received a great deal of attention. Figure 7 shows the flutter dynamic pressure vs the tailoring ply angle for two orthotropic wings and one isotropic wing. In all three cases, body-freedom flutter is critical and small negative ply angles are expected to be effective. There is an implication in Fig. 6 that the low AR wing does not realize much benefit, because its maximum bending stiffness occurs for a somewhat more aft-swept configuration than the other higher AR cases. This fact, demonstrated in Fig. 7, has important implications for the design of low AR wings. If the model used does not account for low AR, then this phenomenon tends to be entirely missed.

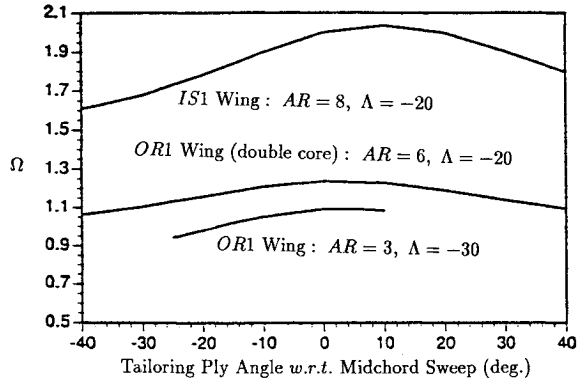


Fig. 6 Frequency parameter vs ply angle.

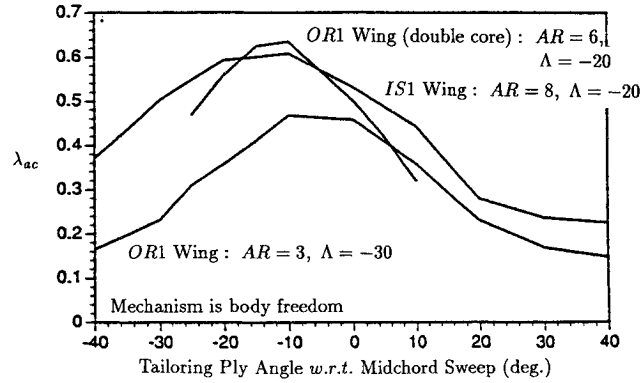


Fig. 7 Flutter dynamic pressure vs ply angle.

Figure 7 shows the interesting and somewhat surprising result that flutter dynamic pressure is strongly affected by very small changes in the layer orientation in the vicinity of 0 deg. Virtually all the analytical and experimental work on tailoring forward-swept wings to date does not consider low AR wings.

Finally, the distribution of tailoring plies over the wing planform is considered. The present model is ideally suited for an investigation of parameters such as layer thicknesses, which are free to vary parametrically in both chordwise and spanwise directions. Such distribution investigations are likely to result in lower structural weight or higher flutter speeds, so that they must be included in any search for an optimal wing design. The present model can be used to conduct such investigations with ease. The results are impressive. In the chordwise direction, a flutter dynamic pressure increase of 25% or decrease of 25% is observed, depending on whether the leading or trailing edge is favored for a linear material distribution, respectively. Similarly, in the spanwise direction, the flutter dynamic pressure increases 29% if the wing root is favored, but drops 35% if the plies are concentrated near the tip. These results are for an OR1 wing of AR 6 and a forward sweep angle of 20 deg. The tailoring layer is swept 10-deg forward of the midchord line. These new results go a long way toward justifying this more sophisticated model.

## VII. Conclusions

At the outset, the goal was to develop a structural model representing a modern aircraft wing sufficiently well and one that is sufficiently simple to be used in a multidisciplinary optimization problem. This goal has been accomplished with the development of a plate model that accounts for shear deformation, variable layer thickness and orientation, fuselage DOFs, and chordwise flexibility. Consistent with conclusions reached by previous investigators, certain factors such as wing camber, unsymmetric ply stacking, and rotatory inertia are sufficiently small for the problem at hand that they can be ignored. The approach developed here should prove valuable in preliminary as well as final analysis. For component evaluation, such as that discussed in the Introduction, the physical characteristics can be described sufficiently well to base design decisions on the results of the analysis.

The algebraic eigenvalue problem was formulated directly from the extended Hamilton principle. In deriving the algebraic eigenvalue problem, the use of recently developed quasi-comparison functions was relied upon to produce a model guaranteeing rapid convergence.

The numerical results obtained by means of the model developed here confirmed various trends established by earlier investigators. They demonstrate that there is a very wide array of interrelated parameters affecting the instability speed. The clearest outcome is a demonstration of the necessity of a formal optimization approach to bring consistency to the investigation of all the pertinent parameters.

The numerical results are limited to demonstration of the various features of the model and to opening forays into regions of investigation previously closed to simpler models. Nevertheless, several previously unreported trends with significant bearing on the design of modern wings were revealed. These initial inquiries open the door to further research and refinement of the concept of composite tailoring. The results indicate that composite tailoring of forward-swept wings may not be nearly as effective for low AR wings as for high AR wings. This is an important result that virtually mandates a structural model of at least the level of sophistication used here to accomplish optimal design of a low AR forward-swept wing.

A second, and also important, new finding pertaining to two-dimensional models is that it pays to tailor ply distributions. Beyond finding the optimum angle of orientation of a tailoring ply, if the distribution is not also subjected to optimization, significant improvements in the flutter speed are forfeited. The results presented here indicate that the tailoring plies are most effective when the distribution favors the leading edge and the wing root. This result is also unobtainable with more conventional models and points once again to the need of sufficient sophistication in modeling. Optimization methods are dictated by a large number of interacting parameters, but such effort is wasted if features affecting the response characteristics are not included in the analytical model.

## Acknowledgments

This work was supported by the AFOSR Research Grant 91-0351, monitored by Spencer T. Wu. This support is greatly appreciated.

## References

[1]Weisshaar, T. A., Zeiler, T. A., Hertz, T. J., and Shirk, M. H., "Flutter of Forward Swept Wings, Analysis and Tests," *Proceedings of the AIAA/ASME/ASCE/AHS 23rd Structures, Structural Dynamics and Materials Conference* (New Orleans, LA), AIAA, New York, 1982, pp. 111–121.

[2]Giles, G. L., "Equivalent Plate Analysis of Aircraft Wing Box Structures with General Planform Geometry," *Journal of Aircraft*, Vol. 23, No. 11, 1986, pp. 859–864.

[3]Giles, G. L., "Further Generalization of an Equivalent Plate Representation for Aircraft Structural Analysis," *Journal of Aircraft*, Vol. 26, No. 1, 1989, pp. 67–74.

[4]Librescu, L., *Elastostatics and Kinetics of Anisotropic and Heterogeneous Shell-Type Structures*, Noordhoff International, The Netherlands, 1977.

[5]Mindlin, R. D., "Influence of Rotatory Inertia and Shear on Flexural Motions of Isotropic, Elastic Plates," *Journal of Applied Mechanics*, Vol. 18, No. 1, 1951, pp. 31–38.

[6]Meirovitch, L., and Kwak, M. K., "Convergence of the Classical Rayleigh-Ritz Method and the Finite Element Method," *AIAA Journal*, Vol. 28, No. 8, 1990, pp. 1509–1516.

[7]Meirovitch, L., *Computational Methods in Structural Dynamics*, Sijhoff and Noordhoff, Alphen aan den Rijn, The Netherlands, 1980.

[8]Bisplinghoff, R. L., and Ashley, H., *Principles of Aeroelasticity*, Dover, New York, 1975.

[9]Moler, C. B., and Stewart, G. W., "An Algorithm for Generalized Matrix Eigenvalue Problems," *SIAM Journal of Numerical Analysis*, Vol. 10, No. 2, 1973, pp. 241–256.

[10]Meirovitch, L., and Kwak, M. K., "Rayleigh-Ritz Based Substructure Synthesis for Flexible Multibody Systems," *AIAA Journal*, Vol. 29, No. 10, 1991, pp. 1709–1719.

[11]Hagedorn, P., "The Rayleigh-Ritz Method with Quasi-Comparison Functions in Non-Self-Adjoint Problems," *Journal of Vibration and Acoustics*, Vol. 115, July 1993, pp. 280–284.

[12]Meirovitch, L., and Hagedorn, P., "A New Approach to the Modeling of Nonself-Adjoint Systems," *Journal of Sound and Vibration*, Vol. 178, No. 2, 1994, pp. 227–241.

[13]Blevins, R. D., *Formulas for Natural Frequency and Modeshape*, Reinhold, New York, 1979.

[14]Rossettos, J. N., and Tong, P., "Finite-Element Analysis of Vibration and Flutter of Cantilever Anisotropic Plates," *Journal of Applied Mechanics*, Vol. 41, No. 4, 1974, pp. 1075–1080.

[15]Stroud, W. J., Dexter, C. B., and Stein, M., "Automated Preliminary Design of Simplified Wing Structures to Satisfy Strength and Flutter Requirements," NASA TN D-6539, Dec. 1971.